ELSEVIER

Journal of Structural Geology 27 (2005) 1346–1354

JOURNAL OF STRUCTURAL GEOLOGY

www.elsevier.com/locate/jsg

Dynamic reverse modelling of flanking structures: a source of quantitative kinematic information

Thomas Kocher*, Neil S. Mancktelow

Geologisches Institut, ETH-Zentrum, CH-8092 Zürich, Switzerland

Received 18 November 2004; received in revised form 18 May 2005; accepted 18 May 2005
Available online 15 July 2005

Abstract

Flanking structures around planar discontinuities in an otherwise homogeneous flow develop a characteristic geometry that is potentially a source of kinematic information about the background flow. Analytical methods were used to calculate the velocity around a thin weak inclusion (representing a fracture) in linear viscous material. This approach allows modelling of flanking structures to very large strains. The velocity field around a given flanking structure can be calculated for the complete range of potential background flow fields, provided that the orientation of the fabric attractor and the bulk shear sense are known. Structures can be undeformed according to these velocity fields and, by quantifying the misfit between the actual and initial geometry, the vorticity number of the flow field and the duration of deformation accurately determined. With these two parameters established, the background (bulk) deformation involved in the formation of a specific flanking structure can be calculated.

Keywords: Dynamic reverse modelling; Flanking structures; Quantitative kinematic information

1. Introduction

Recently much attention has been paid to folding structures that develop around a material discontinuity, first classified as flanking structures by Passchier (2001), but often in the past described as fault drag. The term refers to planar or linear markers, such as a foliation or a stretching lineation (called the host element, HE), which are deflected around a planar material discontinuity (called the cross-cutting element, CE), such as a dyke or a brittle fault. The host element that lies parallel to the symmetry plane of the structure in the far field is called the central marker line (CML). During homogeneous bulk deformation, the presence of the material inhomogeneity induces a heterogeneous strain (called perturbation strain) in the vicinity of the CE, leading to a local deformation and folding of the marker lines. Several papers dealing with this process have been published in the past. One of the first authors to recognise these structures was Hudleston (1989), who described folds associated with discrete fractures in glacial ice. Reches and Eidelman (1995) conducted numerical experiments on the deflection of marker lines around a brittle fracture in elastic material. Passchier (2001) suggested a wide range of mechanisms for the formation of flanking structures around different possible crosscutting elements. However, field observations have established that flanking structures developing around brittle fractures are the most common examples in nature, and therefore research has focused on this particular case. Grasemann and Stüwe (2001) and Grasemann et al. (2003) explored the different types of flanking structures that develop under general transpressive shear. It became clear that the type of structure that develops at small strains mainly depends on the initial orientation of the fracture α_{in} with respect to the bulk flow and on the type of bulk flow itself, i.e. on the kinematic vorticity number W_k (see Means et al., 1980).

Grasemann et al. (2003) proposed a nomenclature system that divides the wide range of flanking structures developed in general shear flow into three classes, namely shear bands, a-type and s-type flanking structures, depending on whether the apparent sense of shear along the CE (given by the offset of the central marker line) is antithetic (a-type) or synthetic (s-type and shear bands) with respect to the bulk sense of shear. Each of these three types can be further subdivided

* Corresponding author. Tel.: +41 1 632 6129; fax: + 41 1 632 1080.
E-mail address: kocher@erdw.ethz.ch (T. Kocher).

0191-8141/$ - see front matter © 2005 Elsevier Ltd. All rights reserved.
doi:10.1016/j.jsg.2005.05.007

into a normal and a reverse structure, depending on whether the sense of rotation of the central marker line at the point where it touches the CE is equal (normal) or opposite (reverse) to the sense of rotation along the CE (see Fig. 1, modified after Wiesmayr and Grasemann (2005)). The same nomenclature is used here. Grasemann et al. (2003) showed that mirror images of flanking structures exist and that these cannot be distinguished if the bulk sense of shear is not known. Reverse a-type flanking structures and reverse shear bands, for example, cannot be discriminated without independent information on the bulk sense of shear. A single flanking structure is therefore not suitable for determining the bulk sense of shear.

Flanking structures associated with brittle fractures are frequently found in calcite–dolomite marbles. However, they also occur in a wide range of other rock types, from high-grade metamorphic gneisses through to sedimentary rocks. Although found in rocks deformed over a wide range of P and T conditions, all these structures have one basic similarity, namely that a brittle fracture developed under generally ductile conditions and that the surroundings subsequently continued to deform in a ductile manner. The host elements outlining the flanking structures are usually defined by layering or foliation. Differences in material properties related to this layering would certainly have an influence on the development of flanking structures. However, most investigated outcrops showed little evidence for important material property differences between marker layers. Besides the folding in the vicinity of the fractures, no folding or cuspate/lobate structures related to such rheological contrasts were observed in the natural examples considered here.

In this paper, we present a semi-analytical method that allows forward modelling of the behaviour of an isolated fracture of finite length in general shear. This method reproduces laboratory experiments and explains the range of different structures that may develop. We demonstrate that dynamic reverse modelling of these structures is also possible. Reverse modelling simply involves making the time step negative, as has previously been reported to be possible for 3-D diapirism (Kaus and Podladchikov, 2001). These tools are then employed to construct an inversion algorithm, which attempts to find a combination of parameters (flow field W_k and time τ), which 'unfolds' the layering. The inversion algorithm is tested against synthetic examples and then applied to natural structures to estimate the flow parameters involved in their formation.

The work by Passchier (2001), Grasemann and Stüwe (2001), Grasemann et al. (2003) and Exner et al. (2004) provides a basic understanding of the development of flanking structures. The results of these studies have shown that flanking structures are not an unambiguous source of kinematic information because of the existence of mirror image geometries. However, if the sense of bulk shear in an outcrop can be determined by independent shear sense criteria (e.g. sigma clasts), then flanking structures can be classified according to Grasemann et al. (2003), and this classification suggests a potential for constraining the W_k of the flow field from the geometry of natural flanking structures. It should be noted, however, that (1) there is an infinite range of combinations of α and W_k, (2) corresponding changes in geometry are quite subtle and require an analysis of the complete geometry and not just particular components, and (3) natural flanking structures are finite strain structures that have evolved with time (cf. Exner et al., 2004). The question remains whether the differences in the finite strain field, expressed by the geometry of marker lines, are sufficient to determine the bulk flow conditions under which the structure formed.

2. Methodology

In this study, analytical methods were used to investigate the development of flanking structures. The brittle fracture embedded in a ductile material was modelled as a thin, weak, linear viscous inclusion embedded in a stronger linear viscous matrix. The assumption of linear viscous behaviour is justified by the numerical results of Grasemann and Stüwe (2001), who found that there is no significant difference in results obtained for linear and power-law viscous rheology. The relevant analytical solution was derived by

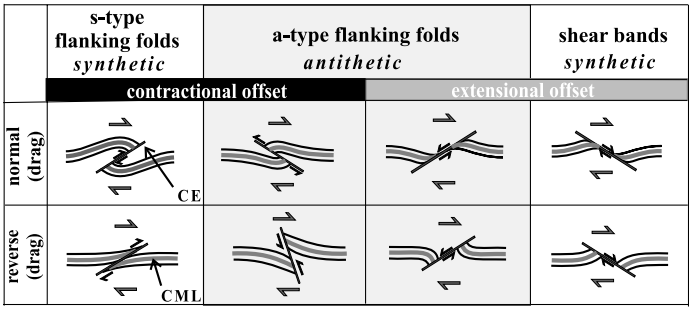

Fig. 1. Nomenclature of flanking structures, modified after Wiesmayr and Grasemann (2005). The sense of shear along the crosscutting element (CE) can be either synthetic or antithetic with respect to the bulk sense of shear. For either case, the drag of the central marker line (CML) may be normal or reverse with respect to the sense of shear along the CE. These four cases may occur with either extensional or contractional offset of the central marker line along the CE, which leads to a total of eight possible flanking structure geometries.

Schmid (2002) and Schmid and Podladchikov (2003). This solution allows the velocity, stress and pressure distribution around an elliptical inclusion of arbitrary orientation to be calculated for any general shear flow field. Both the ellipticity of the inclusion and the viscosity ratio can be chosen in the interval $(1, \infty)$. The approximation of a brittle fracture by a very thin, weak ellipse is therefore possible and any effects caused by the curvature of the hinge of the ellipse may be neglected for large ellipticity values. All experiments in this study were done using an inclusion aspect ratio of 10^7 and a clast/matrix viscosity ratio of 10^{-12}. By introducing marker points around the fracture and applying an implicit time stepping algorithm, flanking structures can be calculated for any flow field W_k and any initial fracture orientation α_{in}, which is the angle between the stretching eigenvector of the flow and the fracture, following the usual mathematical convention (i.e. counter-clockwise positive). Such an analytical method is both very accurate and computationally efficient when compared with numerical methods, such as finite element modelling. There is also no limit to the strain that can be achieved when using analytical methods. However, there is little advantage in calculating results to high strain, because only low strain natural flanking structures can be usefully analysed. With increasing bulk strain, the marker line pattern around the CE quickly becomes so distorted that details of the flanking structure geometry are no longer discernible (Exner et al., 2004).

The analytical solution allows the forward modelling of flanking structures in arbitrary flow fields W_k and for arbitrary initial orientations α_{in}. By simply reversing the flow field, the resultant finite structure can obviously be transformed back into its starting configuration. Such reverse modelling can be used to determine the initial fracture orientation α_{in} and allows the determination of the unknown flow field W_k for an arbitrary flanking structure.

3. Behaviour of flanking structures during progressive deformation

Depending on the initial fracture orientation α_{in} and the flow field, different types of flanking structures develop at small strains (Grasemann et al., 2003). During progressive deformation, these structures rotate, change continuously and may even develop into a different type of flanking structure. Depending on its orientation and the background flow field, the CE rotates at different velocities. However, what is not unequivocally established is whether orientations exist in a particular flow field for which the CE does not rotate at all. In this special orientation, flanking structures that develop would be recognizable over a long period of progressive deformation because of their stable orientation.

The analytical formulations of Schmid (2002) and Schmid and Podladchikov (2003) allow the calculation of velocities at every point along the fracture (represented in two dimensions by a thin, weak elliptical inclusion). These velocities can be factored into fracture-parallel and fracture-perpendicular components. The fracture-parallel components describe the stretching/shortening of the fracture, whereas the components perpendicular to the fracture describe its rotation. If the velocity components perpendicular to the fracture are zero, the fracture does not rotate and only shortening or stretching of the fracture occurs. If any orientation exists where the velocities perpendicular to the fracture are zero at any time during progressive deformation, the fracture will remain in this stable orientation, and subsequently only shortening or stretching of the fracture will occur.

To investigate the rotation behaviour of brittle fractures embedded in linear viscous material, the fracture-parallel and fracture-perpendicular velocities were calculated and the angular velocity $\dot{\omega}$ determined for each point of the fracture. The angular velocities were found to be equal for all points of a fracture, implying that the fracture remains straight during deformation. Fig. 2 shows the normalized rotation rate $\dot{\omega}/\dot{\gamma}$ of the elongate inclusion approximating a fracture in flow field–orientation space. The contour plot shows two straight lines where the rotation rate is zero, which corresponds to the orientation of the eigenvectors of the flow field. Bobyarchick (1986) pointed out that a 2D flow field has two eigenvectors, one being the stretching eigenvector and the other being the shortening eigenvector of the flow. The stretching eigenvector is also called the fabric attractor (Passchier, 1997), because linear structural elements tend to align parallel to this vector during deformation. Fig. 2 shows that single isolated fractures embedded in a linear viscous material have no other stable

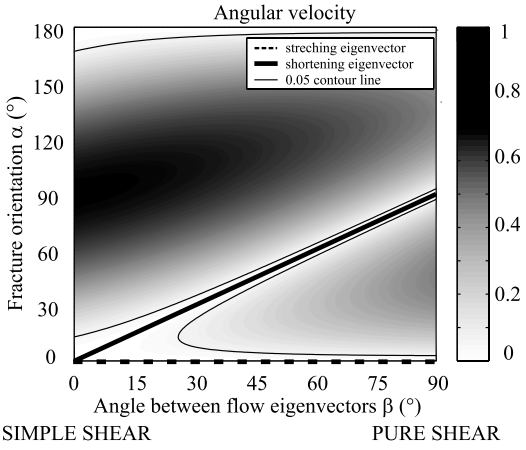

Fig. 2. Angular velocity of a fracture in general shear. The flow type is indicated on the horizontal axis by the angle β between the two flow eigenvectors, which is related to the kinematic vorticity number by the relationship $W_k = \cos(\beta)$. The stretching eigenvector of the flow is kept horizontal in all cases. The fracture rotates fastest when in a 90° orientation in simple shear (with a rotation rate equal to the shear strain rate) and not at all (stable orientation) when parallel to one of the two flow eigenvectors. The overall rotational behaviour is identical to that of a passive marker line.

orientation than those parallel to the flow eigenvectors. Furthermore, the rotational behaviour is the same as that of a passive marker line. With increasing elongation the rotation behaviour of any elliptical inclusion will approach that of a passive marker line, regardless of the viscosity contrast. The difference is already small for an ellipticity greater than 10. Fractures developed in an orientation close to that of an eigenvector rotate very slowly with increasing deformation, and flanking structures that develop in such orientations are therefore preserved over a much wider range of bulk strain. This is a possible explanation for the observation of stable positions in fig. 5 of Grasemann et al. (2003), where experiments were only conducted up to small bulk strains.

4. Dynamic reverse modelling of flanking structures

Grasemann et al. (2003) showed that instantaneously developing structures are not unique with respect to the three parameters that were used in their nomenclature (normal or reverse/a- or s-type/extensional or contractional; see Fig. 1). Instantaneous reverse a-type flanking structures, for example, develop in a wide field of different parameter combinations of vorticity number W_k and initial fracture orientation α_{in} (fig. 6 of Grasemann et al., 2003). However, this observation does not exclude the possibility of determining the flow field and the time that was necessary to form the finite structure if the perturbed geometry around the fracture is considered as a whole. In other words, it is not established if a particular structure is truly unique with regard to the W_k and τ that led to its formation.

To check this hypothesis, an arbitrary flanking structure first developed in a forward model with known (W_k, τ) has been deformed backwards, applying the full range of possible bulk flow fields ($0 \leq W_k \leq 1$). Clearly, the flow field corresponding to that in which the structure was formed must 'undeform' the flanking structure and transform it back into its initial configuration, i.e. all marker lines being straight lines, with no offset along the CE. The important question is how uniquely the (W_k, τ)-parameters can be defined through retro-deformation. If there is only one flow field for which a perfect transformation of the flanking structure into its initial configuration is possible, then the determination is unique and the method may therefore have potential for establishing flow parameters in less tightly controlled natural examples.

In order to independently quantify the correspondence between the initial configuration and the reverse-modelled structure at any time, control lines are introduced by digitizing points along the deflected marker lines of the structure. The straighter these lines, the closer the actual configuration is to the assumed initial configuration. How close they are to the initial configuration can be expressed by introducing a residual R at time τ:

$$R_\tau = \sum_{j=1}^{nlines} \left(\frac{1}{npoints_j} \sum_{i=1}^{npoints_j} \sqrt{\left(y_i(\tau) - y_{mean_j}\right)^2} \right) \quad (1)$$

where j denotes the line index, y_{mean_j} the mean y-position of the line j at time τ, i the point index on the respective line j, $npoints_j$ the number of points in line j, and $nlines$ the total number of digitized marker lines. In order to compare the fit of an actual geometry at time τ to the initial configuration, the residual can be defined as $\Re = R_\tau/R_0$, where R_0 is the residual of the structure at the time $\tau = 0$.

The question whether a specific finite structure corresponds uniquely to a certain flow field and time τ now transforms into the question of finding the minimum of the function $\Re$(flowfield, τ). If this function possesses a well-defined global minimum, then it will be possible to find the correct vorticity number W_k and time τ that formed the flanking structure under consideration. If these two parameters can be uniquely determined, then the bulk deformation matrix D is easily found by

$$D = \begin{pmatrix} \exp\left(\frac{\tau}{2}\sqrt{1-W_k^2}\right) & \frac{2W_k \sinh\left(\frac{1}{2}\tau\sqrt{1-W_k^2}\right)}{\sqrt{1-W_k^2}} \\ 0 & \exp\left(-\frac{\tau}{2}\sqrt{1-W_k^2}\right) \end{pmatrix} \quad (2)$$

modified after Grasemann et al. (2003).

The procedure described above requires knowledge or justified assumptions about the initial configuration of the marker lines. In the case of synthetic flanking structures calculated from forward modelling, the initial orientation of the marker lines are known, i.e. the marker lines were straight and without offset. However, as discussed below (Section 4.3), for natural flanking structures the initial configuration can only be assumed, with the assumption based on the geometry far removed from isolated flanking structures.

4.1. Testing the method on normal s-type flanking structures

Fig. 3 shows an example of an arbitrary synthetic normal s-type flanking structure, calculated using the analytical

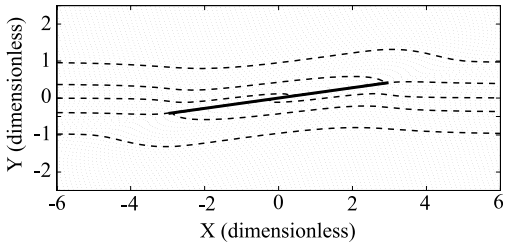

Fig. 3. Example of a normal s-type flanking structure modelled in dextral transpressive shear. The vorticity number W_k was $0.93 = \cos(\beta)$, the initial fracture orientation $\alpha_{in} = 115°$, and the dimensionless time $\tau = 4.20$. The fabric attractor is parallel to the marker lines in the far field (i.e. horizontal across the diagram).

solution for incompressible linear viscous materials. The values of α_{in}, τ and W_k were predetermined but were assumed to be unknowns during the reverse modelling. The only information assumed during reverse modelling was that the marker lines were initially horizontal across the diagram and parallel to the fabric attractor (i.e. the stretching flow eigenvector).

The input for the residual calculation consisted of the (x, y)-coordinates of the marker lines and of the two tip points of the fracture (which is sufficient, since the fracture remains a straight line during deformation). The velocity field around the fracture was then calculated using the analytical solution for every possible flow field and the selected markers and the fracture were moved according to these velocities. At every time step, the residual $\Re$ was calculated and plotted in a two-dimensional diagram, where the horizontal axis refers to the time in dimensionless form (normalized against $2\dot{\varepsilon}_{max}$, which is equal to the stretching factor S in Grasemann et al. (2003)) and the vertical axis refers to angle β between the flow eigenvectors of the applied flow field (where $W_k = \cos(\beta)$). In order to test for (1) the influence of the number of marker lines used to check the reverse calculation, and (2) the influence of digitizing the marker lines and the fracture tips by hand instead of using the calculated values, the residual of the structure in Fig. 3 was calculated twice, once using the marker points of 60 forward-calculated marker lines (Fig. 4), and once using only five marker lines, the coordinates of which were digitized by hand (Fig. 5).

The results of this reverse modelling of the normal s-type flanking structure show a minimum of $\Re$ at $\beta = 21.57°$, $\tau = 4.20$ in both Figs. 4 and 5. To within two decimal point precision, these are exactly the values used in the forward modelling of Fig. 3. For forward and reverse modelling of a perfect synthetic example, the residual should obviously be zero at the minimum. However, the finite time step size and numerical round-off errors result in a still acceptable minimum $\Re$ of ca. 10^{-3} (Fig. 4). The additional error of hand digitizing the coordinates of only five lines results in a minimum $\Re$ of ca. 10^{-2} (Fig. 5). Nevertheless, the values for β and τ corresponding to this minimum are the same to two decimal digits of precision, which is certainly precise enough for our purpose. It is therefore established that in the synthetic example, values of β and τ can be uniquely established by reverse modelling of a flanking structure.

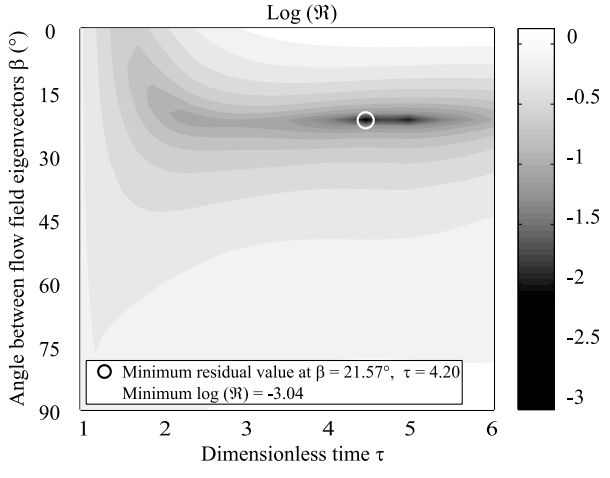

Fig. 4. Residual $\Re$ of the normal s-type flanking structure in Fig. 3. Sixty marker lines were used for reverse calculation and the (x, y)-coordinates of these lines were taken directly from the calculated forward model. The minimum is well-defined in terms of the vorticity number $W_k = \cos(\beta)$, but not for τ.

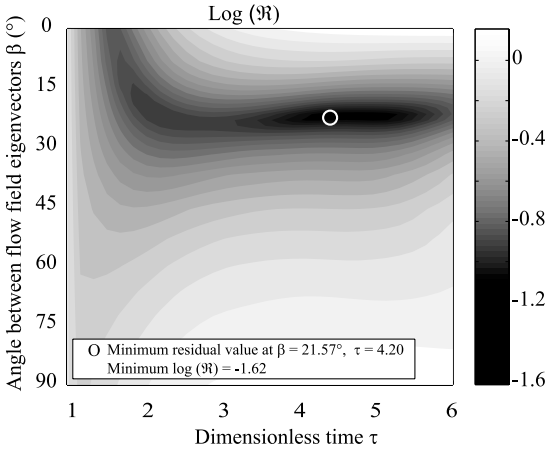

Fig. 5. Residual $\Re$ of the normal s-type flanking structure in Fig. 3. In this case, only the five dashed lines indicated on Fig. 3 were digitized by hand and used in the reverse modelling. The residual $\Re$ is greater than in Fig. 4, due to the error induced by handpicking the points. Nevertheless, the values for β and τ can still be correctly determined.

The residual plots show that the minimum is much better defined for β than for τ. From this it can be deduced that the final geometry is strongly influenced by the type of flow field, but that above a certain strain, the shape of the flanking structure only changes slowly with further deformation.

4.2. Testing the model on reverse a-type flanking structures

Reverse a-type flanking structures are probably the most common examples observed in nature. Grasemann et al. (2003, fig. 6), demonstrated that this type of structure develops over a wide range of parameter combinations of α_{in} and W_k. Reverse a-type flanking structures develop in flow fields with high vorticity numbers as well as in flow fields close to pure shear, and around fractures of strongly varying orientations. Despite this spectrum of boundary and initial conditions, the resulting structures all look very similar, and differences are not immediately obvious. The question posed here is whether three synthetic examples of reverse a-type flanking structures corresponding to different combinations of α_{in}, W_k and τ (Figs. 6–8) are characteristic enough to allow the boundary and initial conditions to be determined by reverse modelling. Taking a close look at the three flanking structures (Figs. 6–8), minor differences in the geometry can be recognized. In particular, the distance

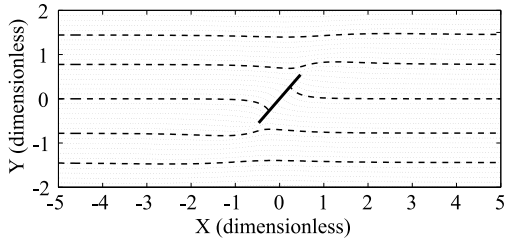

Fig. 6. Reverse a-type flanking structure, formed in a flow field of $W_k = 0.89$ ($\beta = 27.13°$), at $\tau = 1.78$, for $\alpha_{in} = 125°$.

from the CE over which the marker lines are deflected differs for corresponding marker lines in the three examples, as does the change in curvature as a function of distance from the CE. Nevertheless, the differences are small. The reverse modelling procedure was applied to each of the three reverse a-type flanking structures, and a residual calculated and plotted in Figs. 9–11. In each case only the five marker lines and the tips of the fracture were digitized by hand. A global minimum exists for all three examples. According to the residual plot of Fig. 9, the flanking structure in Fig. 6 formed in a flow field with $\beta = 27.13°$ ($W_k = 0.89$), and the deformation lasted for a time of $\tau = 1.78$. In Fig. 10, a flow field of $W_k = 0.62$ and a time $\tau = 1.57$ were found and for Fig. 11, the residual minimum corresponds to $W_k = 0.29$ and $\tau = 1.20$. In all cases, the values are identical to those used in the forward calculation.

However, the minima are not equally well-defined for all three structures. Fig. 9 exhibits a sharp minimum with regard to the flow field, but not time. On the other hand, the minimum of the residual in Fig. 11 is better constrained with respect to τ than the flow field. The residual of the flanking structure in Fig. 7 shows a well constrained minimum for both τ and β, but also the occurrence of a pronounced local minimum for the same flow field, although at a different time.

4.3. Application to natural examples

It is established above that this method can provide quantitative information on well-defined (synthetic) flanking structures. However, the application of this method to natural examples requires certain assumptions to be valid. In the analytical model, it is assumed that all marker lines were straight at the time of fracture formation. This

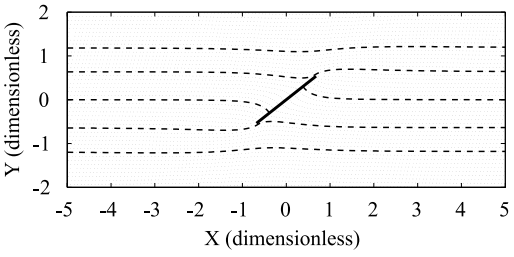

Fig. 7. Reverse a-type flanking structure, formed in a flow field of $W_k = 0.62$ ($\beta = 51.68°$), at $\tau = 1.57$, for $\alpha_{in} = 110°$.

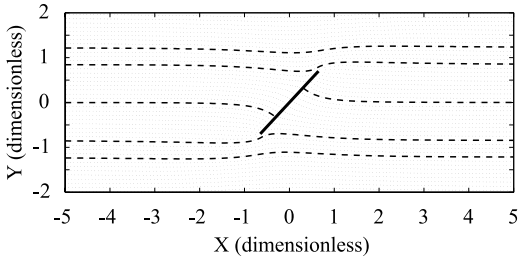

Fig. 8. Reverse a-type flanking structure, formed in a flow field of $W_k = 0.29$ ($\beta = 73.14°$), at $\tau = 1.20$, for $\alpha_{in} = 85°$.

requirement limits the application to rocks which show a relatively undisturbed layering or foliation in areas not affected by the perturbation flow around the fracture. In the far flow field, the stretching eigenvector is also assumed to be parallel to the marker lines at all times. This assumption should hold in nature for the case of strongly sheared zones, where the foliation is assumed to be aligned parallel to the fabric attractor (i.e. the stretching eigenvector). Since flanking structures are mostly small strain structures, the assumption of a constant flow field orientation during the time of formation of the structure is justified. The analytical solution is two-dimensional. An application to natural examples is therefore only possible if the assumption of plane strain is justified on the scale of the flanking structure.

Fig. 12 shows an example of a reverse a-type flanking structure in calcite–dolomite marble from an outcrop in Naxos, Greece. The bulk shear sense of this zone is known to be dextral from independent shear sense indicators. The picture plane of the photograph is oriented perpendicular to the main foliation as well as perpendicular to the fracture surface, and the stretching lineation in the main foliation lies parallel to the plane of the photograph.

The same procedure was applied as described above. The photograph was scanned, the marker lines and the fracture were digitized by hand, and then undeformed using different flow fields W_k. The residual plot is given in Fig. 13. When comparing this residual plot with those of the synthetic examples in the previous section, it is obvious that (1) the minimum is not as well defined as in the synthetic examples,

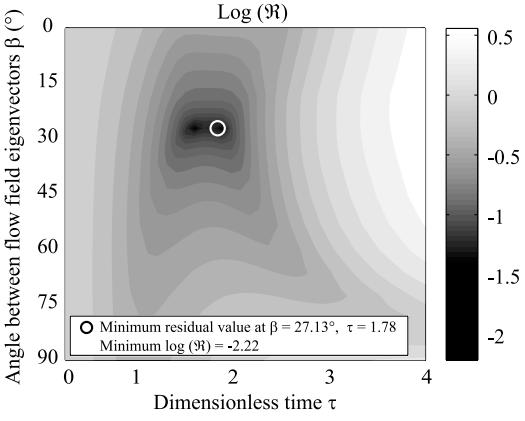

Fig. 9. Residual ℜ of the structure in Fig. 6.

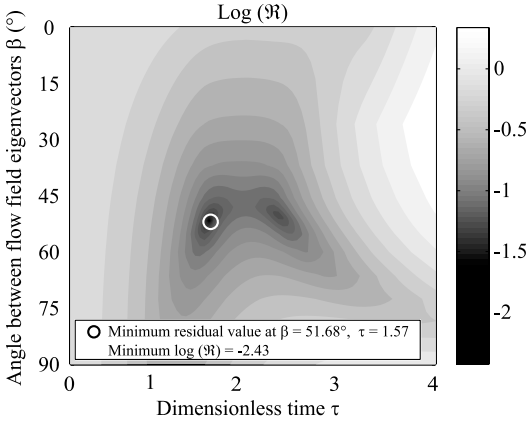

Fig. 10. Residual ℜ of the structure in Fig. 7.

and (2) the value of ℜ is one order of magnitude larger than in the previous examples. The −0.9 contour, which corresponds to a residual of 12% of the initial residual, spans a range of about 30° for β, ranging from 8 to 37°, which corresponds to vorticity numbers between 0.80 and 0.99.

Although the minimum for β is not as tightly constrained as in the synthetic examples, the minimum is still quite well defined. The residual plot therefore does provide a quantitative estimate of the vorticity number W_k of the flow field during formation of this specific flanking structure. Once an estimate of W_k and the time τ is known, the retro-deformation can be visualized by calculating the velocity for every point and incrementally retro-deforming the photograph of the structure (Fig. 14). With progressive retro-deformation, the marker lines are unfolded in the vicinity of the CE, and all lines become straight at a dimensionless time of $\tau \approx 1.2$. Note that not only the most dominant marker line in the middle of the figure, but also the much thinner marker lines that lie closer to the tips of the CE, become horizontal across the diagram. This visualisation clearly shows that the flow field found in the reverse modelling procedure indeed undeforms the flanking structure into an initial configuration in which the marker lines are close to straight and show no offset across the fracture.

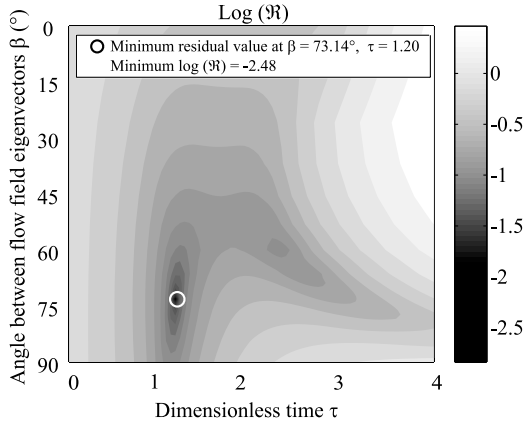

Fig. 11. Residual ℜ of the structure in Fig. 8.

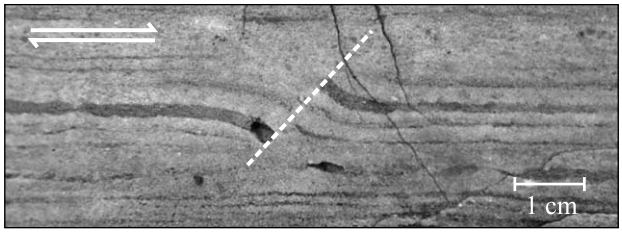

Fig. 12. Reverse a-type flanking structure in alternating mylonitic calcite and more dolomitic (darker) layers from Naxos, Greece (GPS coordinates N37°11′23.6″, E25°30′55.1″, looking WSW). The white arrows indicate the sense of shear, which is dextral (established from independent shear sense criteria).

5. Discussion

Analytical forward modelling demonstrates that a fracture forming the CE of an isolated flanking structure will remain straight and behave like a passive marker line in terms of rotational behaviour. The only orientations for which there is no rotation are those parallel to the eigenvectors of flow. Fractures will rotate toward the stretching eigenvector (the fabric attractor). The orientation parallel to the shortening eigenvector is metastable, because even the smallest deviation away from that orientation will cause the fracture to then rotate toward the fabric attractor. The rotational velocity varies depending on the fracture orientation and a CE that is almost parallel to one of the two flow eigenvectors rotates very slowly; it might therefore be perceived as being stable in numerical and analogue experiments. The rotation of such a CE orientation will only be obvious if high bulk strains are reached. Our analytical results establish that none of the different types of flanking structures has any additional stable position apart from those parallel to the flow eigenvectors. Unstable (i.e. rotating) flanking structures can only be preserved up to moderate amounts of strain. The frequent occurrence of isolated shear bands, for example, can therefore not be explained by stabilization or back-rotation against the bulk

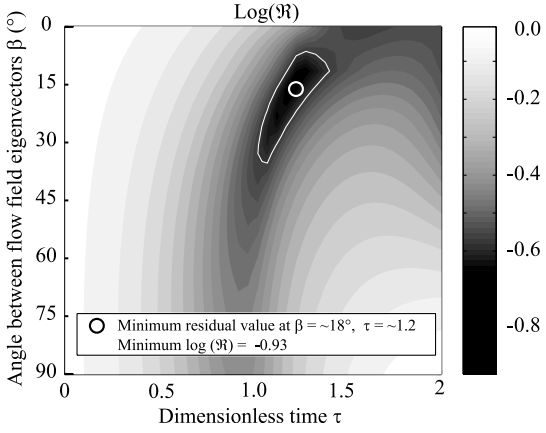

Fig. 13. Residual ℜ of the structure in Fig. 12. The absolute minimum occurs at $\tau = 1.2$, $W_k = 0.95$ ($\beta = 18°$). The contour line is at $\log_{10}(\Re) = -0.9$, which corresponds to a residual of about 12% of the initial residual.

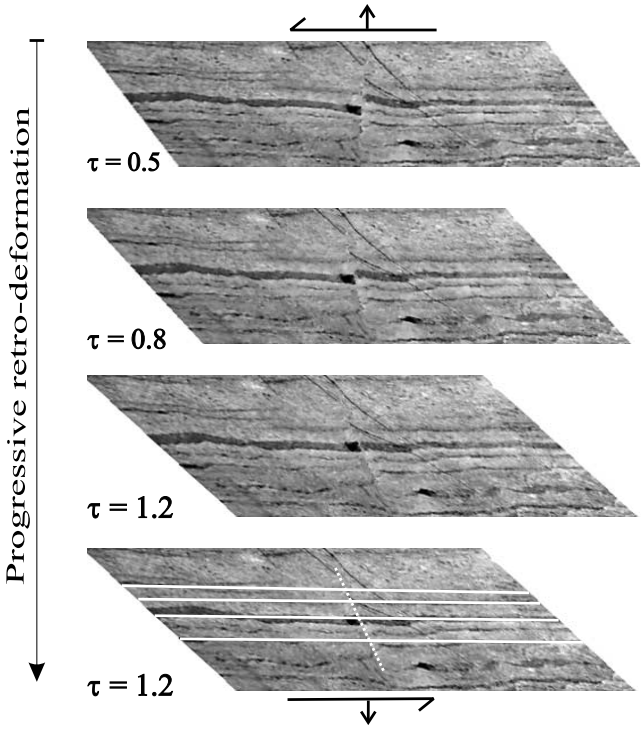

Fig. 14. Retro-deformation of the natural reverse a-type flanking structure from Naxos, Greece (Fig. 12) in a sinistral transtensional flow field (W_k= 0.95). After τ=1.2, the marker lines are approximately straight without offset. The corresponding marker lines are indicated with solid white lines, the position of the fracture with a dotted white line.

sense of shear. The lack of additional stable positions is in contradiction to the numerical results of Wiesmayr and Grasemann (2005), who observed stable positions for CEs oriented at a low angle to the shear plane in simple-shear dominated flow fields.

The reverse modelling experiments performed in this study establish that it is possible to determine the vorticity number W_k of the flow field and the time τ to form a given flanking structure. As soon as W_k and τ are known, the bulk or background deformation D of the material can be calculated. The reverse modelling of synthetic flanking structures previously forward modelled allows a very precise reconstruction of the values of W_k and τ that led to the formation of a particular structure. A comparison of the residual plots reveals that the reconstruction is not equally well constrained for all the flanking structure types analysed in this study. The residual plot of a normal s-type structure exhibits well-constrained minima for the vorticity number W_k, whereas the time τ is less well-constrained (Figs. 4 and 5). This fact is expressed in the elongate shape of the contours, which are aligned parallel to the time axis in the vicinity of the minimum. A slight decrease in W_k causes a strong change in the value of the residual $\Re$. This result indicates that normal s-type flanking structures are most typical of flow fields with a high simple shear component. Grasemann et al. (2003, fig. 6) showed that normal s-type flanking structures only develop in a narrow range of α_{in}–W_k combinations. However, this range also depends on time τ, since normal s-type flanking structures can evolve from reverse a-type flanking structures, as was shown by Exner et al. (2004). As a general observation, it can still be inferred from the residual plot of Fig. 4 that normal s-type flanking structures are typical of simple shear dominated flow fields.

Comparing the three reverse a-type flanking structures shows that they all have well-defined minima for both τ and β (Figs. 9–11). In all three plots, a second local minimum occurs that is variously pronounced. This second minimum develops when a flanking structure is retro-deformed beyond its starting point, so that it rotates further and crosses the instantaneous shortening axis (ISA). This causes a change in the sense of shear along the CE, which reverses the offset acquired between the time point when crossing the true initial orientation and the ISA. The spacing of the minima depends on (1) the rotational velocity of the CE in this range of orientations, and (2) the difference in orientation between the initial fracture orientation α_{in} and the ISA. However, the flow field is the same for both minima and the true minimum has a lower residual and can still be unambiguously determined.

Reverse a-type flanking structures develop for a much wider range of combinations of α_{in} and W_k than normal s-type flanking structures (Grasemann et al., 2003). Reverse modelling of a specific a-type flanking structure at small to intermediate bulk strains therefore produces many more possible combinations of W_k and τ with similar values for the residual $\Re$. Nevertheless, it was possible to determine the exact values of W_k and τ for all three very similar looking structures.

The marker lines record the deformation of the material in the vicinity of the CE. The reverse modelling experiments make use of this information to retrieve the vorticity number W_k. The more characteristic these patterns are, the better is the approximation of the vorticity number. As a general rule, flanking structures that exhibit more complex marker line patterns (many inflexion points along a marker line, fold amplitudes that are large compared with the fracture length) give better results than those with simply bent marker lines. Reverse modelling can be carried out on any marker line affected by the CE. It is only necessary to know the length of the fracture and the far field orientation of the marker line. However, it is not necessary to find the CML, any marker line affected by the CE contains information on the perturbation strain. This is an advantage in the field, because it is often difficult to determine the CML exactly. In the synthetic examples, the use of five single marker lines was already enough to determine both vorticity number W_k and time τ to a high degree of accuracy. For a natural example, all available marker lines should be included in the analysis to obtain the most reliable estimate of the flow field W_k and time τ.

As would be expected, the natural flanking structure example from Naxos, Greece, gave a residual map with a less well-defined minimum than the synthetic examples.

Nevertheless, the flow parameters could be estimated and, as show in Fig. 14, the application of these parameters does indeed produce a retro-deformation of the flanking structure into its assumed initial configuration. The best fit of all marker lines is obtained when deforming the natural example in a flow field of $W_k = 0.95$, which indicates a shear zone parallel stretching at the time of the structure formation (cf. Means, 1989). The assumed initial configuration is achieved after a dimensionless time of $\tau = 1.2$, when no offset remains along the CE and all marker lines are straight and horizontal across the picture.

By reverse modelling the flanking structure, information is also gained on the initial orientation of the fracture. The orientation at $\tau = 1.2$ in Fig. 14 indicates that it formed at an orientation approximately parallel to the orientation of the compressive instantaneous stretching axis (ISA_1), which for isotropic material is itself parallel to the σ_1-axis ($\alpha_{fracture} \approx 65°$, $\sigma_1 \approx 55°$). This suggests that the fracture formed as a mode-I or extensional fracture. The formation of mode-I fractures under upper greenschist to amphibolite facies metamorphic conditions, as is the case for the Naxos example considered here, would require a dramatic reduction of the effective mean stress. An isolated fluid pulse would be one possible trigger for such mode-I brittle fracture in an otherwise ductile rock. This hypothesis is supported by the field observation that several reverse a-type flanking structures, with almost identical orientations of the CE, are developed throughout the outcrops and are apparently of the same age.

The analytical model assumes perfect slip along the fracture surface, with a negligible shear strength of the fracture itself. For the natural example from Naxos, it is difficult to extract any information on the conditions within the fracture during the flanking structure formation. The marbles are now very coarsely recrystallised and no fluid inclusion trails marking the healed fracture could be found in thin section. The presence of the flanking structure itself indicates that continued slip indeed occurred along the fracture. However, the question remains unanswered why the fracture did not heal shortly after it was formed, while the surroundings obviously continued to deform in a ductile way.

6. Conclusions

The reverse modelling experiments have demonstrated that it is possible to place quite tight constraints on the kinematic vorticity number W_k of the bulk flow and the time τ (and therefore the bulk deformation matrix D) involved in the formation of a particular flanking structure. Three similar-looking reverse a-type structures each allowed an accurate determination of the vorticity number and time. These tests on synthetic examples demonstrated that values for these parameters can be extracted even for flanking structures of similar type developed under different conditions. The example of a normal s-type flanking structure provided well-constrained information on the flow field, which suggests that this geometry is typical of simple shear dominated flow. The reverse modelling of a natural a-type flanking structure provided quantitative information on the vorticity number at the time of its formation and allowed a visualisation of this retro-deformation with the finite structure transformed into its assumed initial configuration of straight marker lines and no offset. Flanking structures with well-defined straight fractures (the cross-cutting element CE) and sufficient initially straight markers parallel to the fabric attractor of the far flow field (e.g. mylonitic fabrics in general shear zones) are therefore good potential sources of information on the type of flow field (W_k) and the amount of strain involved in their formation.

Acknowledgements

The Flash team, especially B. Grasemann, G. Wiesmayr, U. Exner and C. Passchier, is thanked for interesting and stimulating discussions. Discussion with B. Kaus on many aspects of numerical modelling and its application is greatly appreciated. D. Schmid helped with implementing the analytical solutions. We thank M. Swanson and J. Hippertt for careful and thorough review of the manuscript. This work was supported by ETH project 0-20998-02.

References

Bobyarchick, A.R., 1986. The eigenvalues of steady flow in Mohr space. Tectonophysics 122, 35–51.

Exner, U., Mancktelow, N.S., Grasemann, B., 2004. Progressive development of s-type flanking folds in simple shear. Journal of Structural Geology 26, 2191–2201.

Grasemann, B., Stüwe, K., 2001. The development of flanking folds during simple shear and their use as kinematic indicators. Journal of Structural Geology 23, 715–724.

Grasemann, B., Stüwe, K., Vannay, J.-C., 2003. Sense and non-sense of shear in flanking structures. Journal of Structural Geology 25, 19–34.

Hudleston, P.J., 1989. The association of folds and veins in shear zones. Journal of Structural Geology 11, 949–957.

Kaus, B.J.P., Podladchikov, Y.Y., 2001. Forward and reverse modeling of the three-dimensional viscous Rayleigh–Taylor instability. Geophysical Research Letters 28, 1095–1098.

Means, W., 1989. Stretching faults. Geology 17, 893–896.

Means, W.D., Hobbs, B.E., Lister, G.S., Williams, P.F., 1980. Vorticity and non-coaxiality in progressive deformations. Journal of Structural Geology 2, 371–378.

Passchier, C.W., 1997. The fabric attractor. Journal of Structural Geology 19, 113–127.

Passchier, C.W., 2001. Flanking structures. Journal of Structural Geology 23, 951–962.

Reches, Z., Eidelman, A., 1995. Drag along faults. Tectonophysics 247, 145–156.

Schmid, D.W., 2002. Finite and infinite heterogeneities under pure and simple shear. PhD thesis No. 14855, ETH Zürich.

Schmid, D.W., Podladchikov, Y.Y., 2003. Analytical solutions for deformable elliptical inclusions in general shear. Geophysical Journal International 155, 269–288.

Wiesmayr, G., Grasemann, B., 2005. Sense and non-sense of shear in flanking structures with layer-parallel shortening: implications for fault-related folds. Journal of Structural Geology 27, 249–264.